FERMILAB-CONF-19-380-AD

Theory and conceptual design of stripline kickers

Yisheng Tu[1], Tanaji Sen[2], and Jean-Francois Ostiguy[2]

[1] *University of Rochester, Department of Physics and Astronomy*
[2] *Fermi National Accelerator Laboratory, Accelerator Division*

Lee Teng Internship, summer 2019

Contents

This manuscript has been authored by Fermi Research Alliance, LLC under Contract No. DE-AC02-07CH11359 with the U.S. Department of Energy, Office of Science, Office of High Energy Physics.

Abstract

In this project we design dipole and quadrupole stripline kickers for echo generation in the IOTA ring. We developed a semi-analytic solver for dipole and quadrupole kickers with curved plates of infinitesimal thickness, and independently validated it against a finite element software code (FEMM). The analytic series converges rapidly and is in agreement with FEMM within 5% everywhere except at the tips of the plates. We also consider finite thickness plates of different shapes (curved and parallel) and compare the central field quality and characteristic impedance. We find that in the dipole case, the parallel plates provide better field quality than curved plates while in the quadrupole case, the difference is not significant. The characteristic impedance of relevant modes are computed. Matching the characteristic impedance to an external load is necessary to prevent unwanted reflection and ringing.

1 INTRODUCTION

When beam motion is driven for a finite amount of time, as soon as the excitation is turned off, the envelope oscillation decoheres because individual particles oscillate at slightly different betatron frequencies. Beam echo is a phenomenon whereby a particle beam is successively subjected to two coherent excitation pulses and the motion driven by the initial excitation recoheres at a later time. The phenomena is useful as a diagnostic to extract information about non-linearties and other sources of phase-space diffusion. In the Integrable Optics Test Accelerator (IOTA) ring, dipole and quadrupole stripline kickers produce electromagnetic pulses to coherently drive the beam in a controlled manner, so as to produce echoes. To prevent unwanted reflections and ringing, the characteristic impedance of the kickers must be properly matched.

Each kicker type (dipole or quadrupole) is a multi-conductor shielded transmission line. The dipole configuration has two normal modes and the quadrupole has four. For the dipole configuration, the two modes are the "even" (or symmetric) mode, with both plates at the same potential; and the "odd" (or anti-symmetric) mode where the voltages are of equal magnitude and opposite signs. Of the four quadrupole configuration modes, two produce a dipole field and are not relevant here. The other two have all plates at the same potential ("sum" mode) or adjacent plates at opposite potentials ("quadrupole" mode). The even mode in the dipole kicker and sum mode in the quadrupole kicker are excited by the particle beam which induces charge of opposite sign to the beam on all plates. Unless these modes are properly matched, the kicker will behave as a resonator excited by the circulating particle beam, leading to possible instabilities at high enough beam current. Each mode has a specific spatial distribution of electromagnetic fields and therefore a specific characteristic impedance. We study the modes separately. A schematic for each case is shown in Figure 1.

The main goal of this work is to develop a concept for kickers that can fit into the IOTA ring and used to generate echoes with good quality echoes. Due to the limited space available in the ring, we require our kickers to be compact. The dipole kickers should have a strong, uniform central electric field while the quadrupole kickers should have a strong central field gradient. Finally, the characteristic impedance(s) of the relevant transmission line mode(s) must be properly matched.

In Sec. 2 and 3, we develop the theory for dipole and quadrupole stripline kicker respectively. In Sec. 4, we compare the results obtained from our semi-analytic solver to those obtained with the Finite Element Method Magnetics (FEMM), a purely numerical finite element code. In Sec. 5, we compare how different kicker electrode shapes meet the requirements. We conclude in Sec. 6

2 DIPOLE STRIPLINE KICKER THEORY

2.1 Dipole configuration: odd mode

The derivation in this section and in the next section follows the one in [1].
Consider the dipole electrode configuration shown in Figure 1. The plates are assumed to be infinitesimally

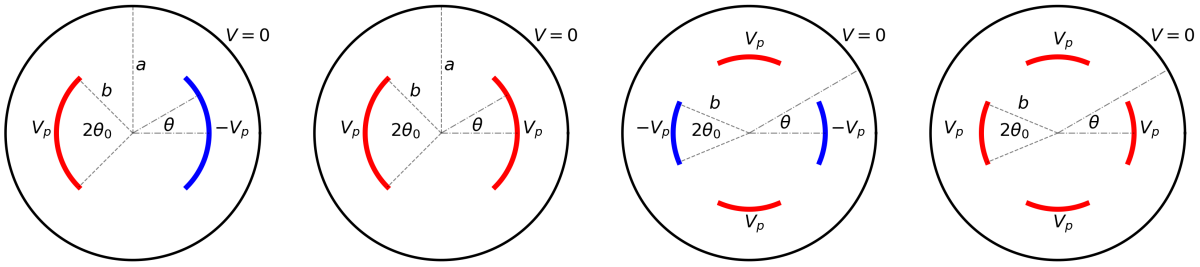

Figure 1: Schematic for the semi-analytic solvers. From left to right: dipole odd mode, dipole even mode, quadrupole mode, quadrupole sum mode. The dimensional parameters a b, θ_0, θ are defined as shown; color red denotes potential held at $+V_p$, blue denotes potential held at $-V_p$ and black denotes potential held at $V = 0$.

thin. The left plate is held at potential V_p, the right at potential $-V_p$ and the beam pipe is held at $V = 0$ at all times.
Because there is no charge in the region interior and exterior to the plates, the potential follows Laplace's equation

$$\nabla^2\Phi = 0 \tag{1}$$

In 2D polar coordinates, the general solution is

$$\Phi(r,\theta) = a_0 \ln(r) + b_0 + \sum_{m=1} [a_m r^m + b_m r^{-m}][c_m \cos m\theta + d_m \sin m\theta] \tag{2}$$

To solve for the potential, we divide the problem domain into two regions. Denote the potential in the region $0 \le r \le b$ as Φ_{in}, and in the region $b \le r \le a$ as Φ_{out}.
The potential is subject to the following boundary conditions (B.C.) for the odd mode:

1. Φ is finite at $r = 0$: $\Phi(0,\theta) < \infty$
2. $\Phi = 0$ at $r = a$: $\Phi(a,\theta) = 0$
3. The potential is continuous across each plate: $\Phi_{\text{in}}(b,\theta) = \Phi_{\text{out}}(b,\theta)$
4. The radial derivative of the potential is continuous in the gaps between the plates: $\frac{\partial\Phi_{\text{in}}}{\partial r}|_{r=b} = \frac{\partial\Phi_{\text{out}}}{\partial r}|_{r=b}$
5. The potential is prescribed on each plate

In addition, for each case at hand, symmetry about x axis ($\Phi(r,\theta) = -\Phi(r,-\theta)$) implies $d_m = 0$ and anti-symmetry about y axis ($\Phi(r,\theta) = \Phi(r,2\pi-\theta)$) implies that m must be an odd integer.
First, consider the interior region. By B.C. 1, $a_0 = b_m = 0$. Absorbing a_m into c_m, we get

$$\Phi_{\text{in}} = \sum_{m=1,3,..} c_m r^m \cos m\theta \tag{3}$$

The solution in the exterior region is distinct from inner solution, so are the coefficients. Consider the region outside the electrodes. The series coefficients differs from those of the inside region. Denote these coefficients by $A_0, B_0, A_m, B_m, C_m, D_m$ in the same order as in equation 2. By B.C. 2, $B_0 = -A_0 \ln(a)$; $B_m = A_m a^{2m}$. By symmetry, $A_0 = D_m = 0$ and m must be odd. Absorbing redundant coefficients, one gets

$$\Phi_{\text{out}} = \sum_{m=1,3,...} A_m \left(r^m - \frac{a^{2m}}{r^m}\right) \cos m\theta \tag{4}$$

Now using B.C. 4, we can express A_m in terms of c_m

$$A_m = \frac{c_m}{1-(a/b)^{2m}} \tag{5}$$

Define

$$X_m = \frac{b^m c_m}{V_p} \qquad \text{and} \qquad g_m = \frac{1}{1-(b/a)^{2m}}$$

Imposing all boundary conditions, we can write the potential as

$$\begin{aligned} \Phi_{\text{in}}(r,\theta) &= V_p \sum_{m=1,3,..} X_m \big(\frac{r}{b}\big)^m \cos m\theta \\ \Phi_{\text{out}}(r,\theta) &= V_p \sum_{m=1,3,...} \frac{X_m}{1-(a/b)^{2m}} \Big[\big(\frac{r}{b}\big)^m - \big(\frac{a^2}{rb}\big)^m\Big] \cos m\theta \end{aligned} \tag{6}$$

Evaluating the potential at $r = b$, we obtain two equations for the series coefficients X_m.

$$\sum_{m=1,3,...} X_m \cos m\theta = -1 \tag{7}$$

$$\sum_{m=1,3,...} m g_m X_m \cos m\theta = 0 \tag{8}$$

These equations must be simultaneously satisfied.

2.1.1 General description of methods for determining series coefficients

Two methods were used to determine the coefficients X_m. The first method is referred to as the "least squares method". We construct a quadratic "error function"

$$\text{Err}(X_m) = \int_{-\theta_0}^{\theta_0} \big[1 + \sum_{m=1,3,...} X_m \cos m\theta\big]^2 d\theta + \int_{\theta_0}^{\pi-\theta_0} \big[m g_m X_m \cos m\theta\big]^2 d\theta \tag{9}$$

We then seek the set of X_m that minimizes this error function. Taking partial derivatives with respect to X_m and equating the results to zero yields the matrix equation

$$\sum_{n=1,3,...} B_{mn} X_m = -b_n \qquad \text{n odd} \tag{10}$$

where

$$B_{nn} = A_{nn} + n^2 g_n^2 \Big(\frac{\pi}{2} - A_{nn}\Big)$$

$$B_{mn} = \big[1 - mn g_m g_n\big] A_{mn}$$

$$b_n = \frac{2}{n} \sin n\theta_0$$

and

$$A_{nn} = \theta_0 + \frac{1}{2n} \sin 2n\theta_0$$

$$A_{mn} = \frac{\sin(m-n)\theta_0}{m-n} + \frac{\sin(m+n)\theta_0}{m+n}$$

This matrix equation (10) must be truncated and solved numerically.

The second method is referred to as the "projection method". In this case the potential function is projected on a set of basis function ($\cos m\theta$). Each boundary condition at $r = b$ yields a matrix equation; both equations need to be satisfied simultaneously. They are

$$\sum_{m=1,3..} A_{mn}X_m + b_n = 0 \tag{11}$$

and

$$ng_n\Big(\frac{\pi}{2} - A_{nn}\Big)X_n - \sum_{m=1,3..\neq n} mg_m A_m nX_m = 0 \tag{12}$$

Combining equation 11 and 12, we obtain

$$C_{nn}X_n + \sum_{m=1,3,...\neq n} C_{mn}X_m = -b_n \tag{13}$$

where b_n is defined above, and

$$C_{nn} = (1 + ng_n)A_{nn} - n\frac{\pi}{2}g_n$$

$$C_{mn} = (1 + mg_m)A_{mn}$$

The system (equation 13) must be truncated and solved numerically.

2.1.2 Characteristic impedance

Further details can be found in [1]; we present here only the basic method and the result.

The characteristic impedance is defined as

$$Z_c = \frac{V_p}{I_p} \tag{14}$$

where V_p and I_p are the voltage and the current respectively on one of the plates. Since V_p is known, we only need to obtain an expression for I_p. The surface current density K_p is given by

$$K_p = \frac{1}{Z_0}\big[E_{\text{in,r}}(r = b) - E_{\text{out,r}}(r = b)\big] \tag{15}$$

where Z_0 is the vacuum impedance, $E_{\text{in,r}}, E_{\text{out,r}}$ are the radial electric fields internal and external to the plates respectively. Thus I_p is the integral over the entire plate.

$$I_p = \int K_p ds = b\int_{-\theta_0}^{\theta_0} K_p d\theta \tag{16}$$

For the odd transmission mode, the characteristic impedance is found to be

$$Z_c = \frac{Z_0}{|\sum_{m=\text{odd}} X_m g_m \sin m\theta_0|} \tag{17}$$

Matching this characteristic impedance to the external environment is necessary to minimize unwanted reflections.

2.2 Dipole configuration: even mode

We start with Laplace's equation again, the general solution to Laplace's equation still holds (equation 2) as well as boundary condition 1-5. However, the potential is now symmetric with respect to the vertical axis (y axis) and therefore, m must be even.

Using the method described above, we get constraints on the coefficients. As before, introduce

$$X_0 = \frac{c_0}{V_p} \qquad \text{and} \qquad X_m = \frac{b^m c_m}{V_p}$$

We get the expression of the inside and outside potential solutions after satisfying all the boundary conditions as

$$\Phi_{\text{in}} = V_p \sum_{m=0,2,4,..} X_m \big(\frac{r}{b}\big)^m \cos m\theta \tag{18}$$

$$\Phi_{\text{out}} = V_p \Big[X_0 \frac{\ln(r/a)}{\ln(b/a)} + \sum_{m=2,4,..} \frac{X_m}{1-(a/b)^{2m}} \big[\big(\frac{r}{b}\big)^m - \big(\frac{a^2}{rb}\big)^2 \big] \cos m\theta \Big] \tag{19}$$

Again using B.C. 5 and 6, we obtain two equations for the X_m as

$$\sum_{m=0,2,...} X_m \cos m\theta = 1 \tag{20}$$

$$X_0 - 2\ln\left(\frac{b}{a}\right) \sum_{m=2,4,...} m g_m X_m \cos m\theta = 0 \tag{21}$$

The resulting matrix equations using the least squares and projection methods have a similar form to those for the odd mode and can be found in [1].

2.2.1 Characteristic impedance

The characteristic impedance is found to be

$$Z_c = \frac{Z_0}{\pi} \frac{\ln(a/b)}{|X_0|} \tag{22}$$

3 QUADRUPOLE STRIPLINE KICKER THEORY

3.1 Quadrupole mode

The general solution Laplace's equation and the boundary conditions still hold. However, the symmetries are different.

- The potential is symmetric about y axis: $\Phi(r, \pi - \theta) = \Phi(r, \theta)$
- The potential is symmetric about x axis: $\Phi(r, \theta) = \Phi(r, -\theta)$
- The potential is anti-symmetric about $y = x$ (diagonal): $\Phi(r, \frac{\pi}{2} - \theta) = -\Phi(r, \theta)$
- The potential is anti-symmetric about $y = -x$: $\Phi(r, \frac{\pi}{2} + \theta) = -\Phi(r, \pi - \theta)$

0 Using the same method as in the preceding sections, matching the interior and exterior solutions and introducing X_m as defined above, we get

$$\Phi_{\text{in}} = V_p \sum_{m=2,6,10...} X_m \big(\frac{r}{b}\big)^m \cos m\theta \tag{23}$$

$$\Phi_{\text{out}} = V_p \sum_{m=2,6,10...} \frac{X_m}{1-(a/b)^{2m}} \Big[\big(\frac{r}{b}\big)^m - \big(\frac{a^2}{rb}\big)^m\Big] \cos m\theta \tag{24}$$

Applying B.C. 7 and 8, we get

$$\sum_{m=2,6,10...} X_m \cos m\theta = 1 \tag{25}$$

$$\sum_{m=2,6,10...} m g_m X_m \cos m\theta = 0 \tag{26}$$

The matrix equations to numerically determine the coefficient X_m can be obtained by using either one of the methods described in Sec. 2.1.1.

3.1.1 Characteristic impedance

Using once again using the method described in [1], the characteristic impedance for the quadrupole mode is found to be

$$Z_c = \frac{Z_0}{|\sum_{m=2,6,10...} X_m g_m \sin m\theta_0|} \tag{27}$$

3.2 Quadrupole sum mode

In this case the symmetries are as follows:

- The potential is symmetric about $y = x$ (diagonal): $\Phi(r, \frac{\pi}{2} - \theta) = \Phi(r, \theta)$
- The potential is symmetric about $y = -x$: $\Phi(r, \frac{\pi}{2} + \theta) = \Phi(r, \pi - \theta)$
- The potential is the same on the plate for both inside and outside solution: $\Phi_{\text{in}}(b, \theta) = \Phi_{\text{out}}(b, \theta) = V_p$ over all plates

Using the boundary conditions we get the potential

$$\Phi_{\text{in}} = V_p \Big[X_0 + \sum_{m=4,8...} X_m \big(\frac{r}{b}\big)^m \cos(m\theta)\Big] \tag{28}$$

$$\Phi_{\text{out}} = V_p \Big[X_0 \frac{\ln(r/a)}{\ln(b/a)} + \sum_{m=4,8...} \frac{X_m}{1-(a/b)^{2m}} \big[\big(\frac{r}{b}\big)^m - \big(\frac{a^2}{rb}\big)^m\big] \cos m\theta\Big] \tag{29}$$

Applying the boundary conditions on the plates, we get

$$\sum_{m=0,4,8...} X_m \cos m\theta = 1 \tag{30}$$

$$X_0 - 2\ln\left(\frac{b}{a}\right) \cdot \sum_{m=0,4,8...} m X_m g_m \cos m\theta = 0 \tag{31}$$

Matrix equations to determine the X_m may once again be determined by using either the projection or least squares method [1].

3.2.1 Characteristic impedance

The characteristic impedance for the sum transmission mode is found to be

$$Z_c = \frac{2Z_0}{\pi}\frac{\ln(b/a)}{|X_0|} \tag{32}$$

4 NUMERICAL SOLUTIONS FOR THE SOLVER

The (truncated) $N \times N$ matrix equations are solved with linalg.solve method from the python scipy package. We also tested the QR and SVD algorithm; the results were essentially the same as the generic linalg.solve method.

Sample results are presented in figure 2 for the dipole kicker odd mode and in figure 3 for the dipole kicker even mode and two modes in the quadrupole kicker.

In figure 2, we conducted a convergence study for different kicker geometries. The results indicate that good convergence is achieved with ~ 200 terms, In the case $\theta_0 = 0.25\pi$, with 200 terms the relative error is $\leq 5\%$ almost everywhere on the plane except at the tips of the plate; increasing the number of terms to 300 terms yields no significant change. In general, better agreement with FEMM is observed as the plates angular span increases. For plates with small angular span, the result differs from those obtained with FEMM by $\sim 6\%$ almost everywhere on the plate surface.

The fact that the relative error along a symmetry line is always $\sim 100\%$ is caused by the fact that the potential is 0.

Figure 3 shows error distribution for the dipole even mode, the quadrupole mode and the quadrupole sum mode. The relative error generally $< 5\%$ everywhere except in the vicinity of the electrodes tips.

5 KICKER DESIGN WITH FEMM

Finite Element Method Magnetic (FEMM) is a free, open source program [2]. It can solve magneto-static and electrostatics problems, heat flow and low-frequency time harmonic electromagnetic problems. The 2D problem region is subdivided into triangular nodal finite elements. The program solves for the potential at the element nodes and interpolates to get the values everywhere within the problem definition. For this project, we used both electrostatic and magneto-static solvers, although in principle only the electrostatic solver is required since the electric and magnetic fields of a TEM wave are both orthogonal and proportional to each other.

5.1 Characteristic impedance with FEMM theory

The characteristic impedance is defined as

$$Z_c = \frac{V_c}{I_c} \tag{33}$$

where V_c is the potential on one electrode and corresponding I_c is the total current on one electrode. Because FEMM cannot output V_c and I_c at the same time, we need to convert the variables we can obtain from FEMM.

Some useful relations:

$$E_E = \frac{1}{2}CV^2 \quad \text{and} \quad \mathscr{E}_E = \frac{1}{2}\epsilon_0 E^2 \qquad E_B = \frac{1}{2}LI^2 \quad \text{and} \quad \mathscr{E}_B = \frac{1}{2\mu_0}B^2$$

where E_E is total energy stored in the electric field, C is the capacitance, V is voltage; $\mathscr{E}_E$ is the electric field energy density, E is the electric field magnitude; E_B is the total energy stored in the magnetic field,

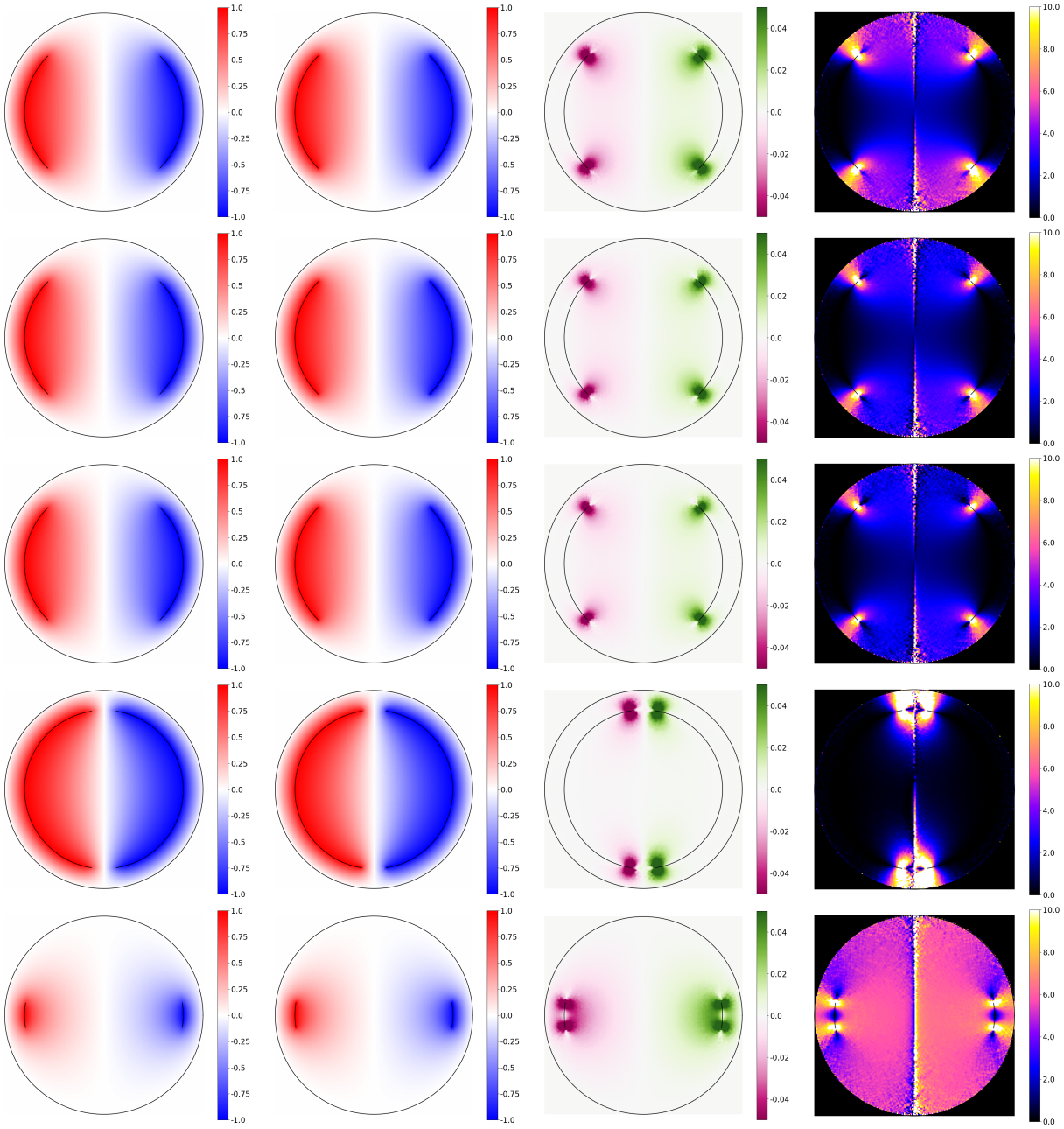

Figure 2: Dipole odd mode comparison. The black lines in all figures are the beam pipe and kicker plates. In all cases we used the projection method and $\frac{b}{a} = 0.8$. In the first three rows $\theta_0 = 0.25\pi$; the number of terms is 100, 200 and 300 terms for the first, second and third row respectively. In the fourth row $\theta_0 = 0.45\pi$, with 200 terms; in fifth row $\theta_0 = 0.05\pi$, with 200 terms. The first column is the analytic solution; the second column is the solution obtained with FEMM; the third column is the difference between the semi-analytic and FEMM solutions and the fourth column is the corresponding relative error.

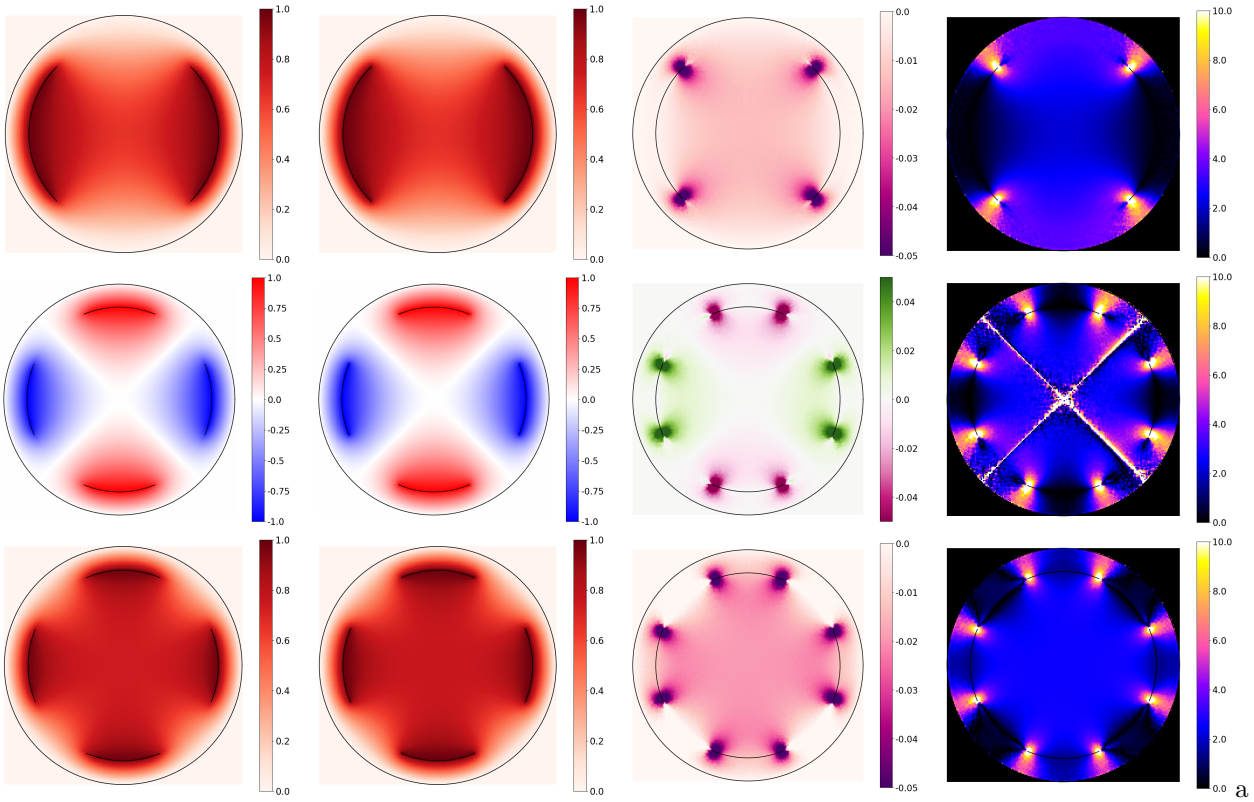

Figure 3: First row: Dipole even mode comparison; second row: quadrupole mode; third row: quadrupole sum mode. The column ordering is the same as in figure 2. The analytic solution behavior is similar to the odd analytic solution. With good agreement ($< 5\%$ difference) everywhere on the plate except near the tips.

L is the inductance, I is the current; $\mathscr{E}_B$ is the magnetic field energy density and B is the magnetic field magnitude. In a transmission line, a propagating TEM wave obeys

$$\frac{E}{B} = c$$

where c is the speed of light.
We also know that by solving the wave equation, $\frac{1}{\sqrt{L'C'}}$ is the wave speed where L', C' are the inductance per unit length and capacitance per unit length respectively. In this case, the wave speed is the speed of light. So

$$\frac{1}{\sqrt{L'C'}} = c$$

In addition, we know that

$$\oint Hdl = I_{\text{enclosed}}$$

where H is the magnetic field strength.

The quantities available in FEMM for electrostatic problems are E, E_E; the quantities available for magneto-static problems are B, H, E_H.

One way to compute the characteristic impedance is by converting the problem to an electrostatic-only

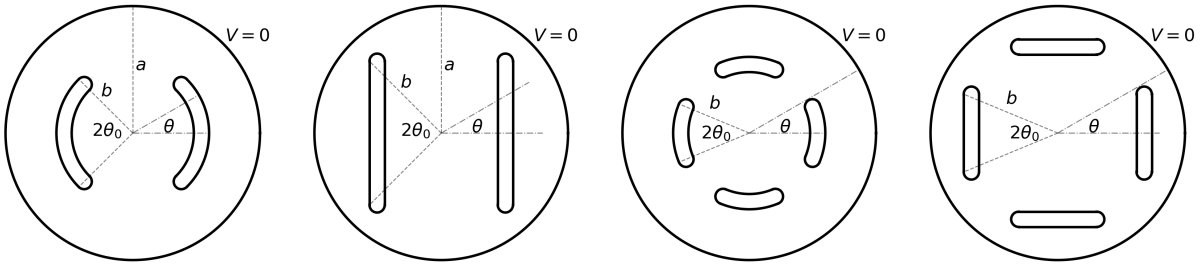

Figure 4: Schematic of the shapes under consideration. Note that for the parallel plates, b is defined to be the distance from the center to the top or bottom edge of a plate, so the distance from beam-pipe center to center of a plate is $d = b\cos\theta_0$.

problem. In this case if V_c and I_c are matched (E and B are matched), then we have

$$\frac{E_E}{E_B} = \frac{\int \mathscr{E}_E d\tau}{\int \mathscr{E}_B d\tau} = \frac{\int \frac{1}{2}\epsilon_0 E^2 d\tau}{\int \frac{1}{2\mu_0} B^2 d\tau} = \frac{\int \frac{1}{2}\epsilon_0 (Bc)^2 d\tau}{\int \frac{1}{2\mu_0} B^2 d\tau} = \frac{c^2}{1/(\mu_0\epsilon_0)} = \frac{c^2}{c^2} = 1$$

Thus we can rewrite characteristic impedance as

$$Z_c = \frac{V_c}{I_c} = \sqrt{\frac{2E_E}{C}}\sqrt{\frac{L}{2E_B}} = \sqrt{\frac{E_E}{E_B}\frac{L}{C}} = \sqrt{\frac{L}{C}} = \sqrt{\frac{L'}{C'}} = \sqrt{\frac{1}{c^2(C')^2}} = \frac{1}{cC'} = \frac{V^2 l}{2cE_E} \tag{34}$$

where l is the conductor length.

Another way is to use a electrostatic and a separate magneto-static problem to compute a set of V, E_E and I, E_B. Then use a relation to pair I to V. We know that C and L are related to the electric and magnetic energies

$$C = \frac{2E_E}{V^2} \qquad \text{and} \qquad L = \frac{2E_B}{I^2}$$

Because C and L only depend on the geometry, no matter what current/voltage are in the system, they are constants. Therefore

$$\frac{2E_{E1}}{V_1^2} = C = \frac{2E_{E2}}{V_2^2} \qquad \text{and} \qquad \frac{2E_{B1}}{I_1^2} = L = \frac{2E_{B3}}{I_3^2}$$

where each subscript denotes a different $V - I$ combination.
Rearranging, we get

$$V_1 = \sqrt{\frac{E_{E1}}{E_{E2}}}V_2 \qquad \text{and} \qquad I_1 = \sqrt{\frac{E_{B1}}{E_{B3}}}I_3$$

Substituting these into equation 33

$$Z_c = \frac{V_1}{I_1} = \sqrt{\frac{E_{E1}}{E_{E2}}}V_2\sqrt{\frac{E_{B3}}{E_{B1}}}\frac{1}{I_3} = \sqrt{\frac{E_{E1}}{E_{B1}}}\sqrt{\frac{E_{B3}}{E_{E2}}}\frac{V_2}{I_3} = \sqrt{\frac{E_{B3}}{E_{E2}}}\frac{V_2}{I_3} \tag{35}$$

This equation relates the characteristic impedance to the voltage and electric field energy in a configuration (2) with the current and magnetic field energy in a separate and unrelated configuration (3). These two methods are used to check for self-consistency.

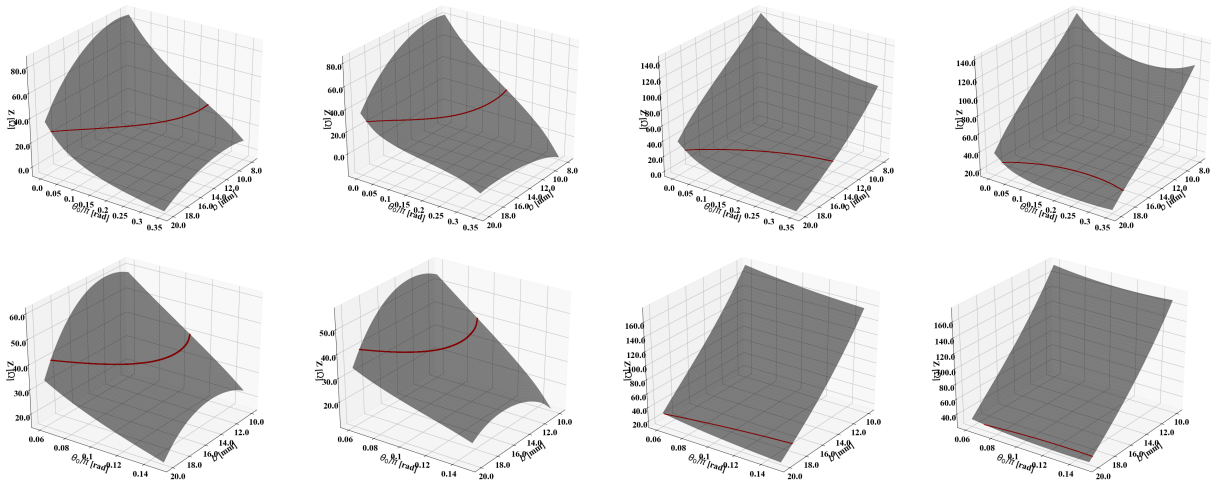

Figure 5: All figures: horizontal axis are θ_0 and b respectively. Vertical axis is Z, the characteristic impedance. Fist row, from left to right: dipole curved odd mode, dipole parallel odd mode, dipole curved even mode, dipole parallel even mode. Second row, from left to right: quadrupole curved mode, quadrupole parallel mode, quadrupole curved sum mode, quadrupole parallel sum mode. The red line shows the intersection of the surface with the $Z = 50\Omega$ line.

5.2 Problem definition and setup

A schematic of the setups is shown in figure 4. We name the setups "dipole curved", "dipole parallel", "quadrupole curved", "quadrupole parallel" from left to right respectively. Dimensions of the kicker are defined using variables in the figure. We consider two modes of operation for each kicker (just as before).

For reasons stated in the introduction, we want to find the highest uniform central electric field (dipole) and electric field gradient (quadrupole) while matching the characteristic impedance of the kicker to the external systems. To do so we first find the parameter space where the characteristic impedance is close to external systems (in our case $Z_{\text{ext}} = 50\Omega$), then choose the configuration to match our requirements.

5.3 Parameter space of matched characteristic impedance

Using the equations for the characteristic impedance mentioned earlier, we computed the characteristic impedance for the parameter space of b, θ_0 and thickness. The characteristic impedance dependence on thickness is much weaker then the dependence on b and θ_0. For this study, we assume a fixed thickness and discuss the effect of varying thickness at the end. For the rest of the section (except the last), we assume thickness = 3mm; $a = 25$mm.

The parameter space we scan and the values of Z_c are shown in figure 5. The figures show Z_c as a function of b and θ_0. We take 10 sample points per parameter (100 sample points total) to interpolate. The intersection is determined within 1.0Ω of $Z_c = 50\Omega$. The red line projection on the $b - \theta_0$ surface is shown in figure 6. Let us point out a few features from the plots in Fig. 6. The even dipole mode allows a smaller range of θ_0 values and requires $b \geq 17$mm compared to the odd mode, the allowed range in b is smaller for the parallel plate case. Similarly for the quadrupoles, matching the characteristic impedance in the sum mode is only possible over a relatively narrow range of b values, the range being narrower still for the parallel plates.

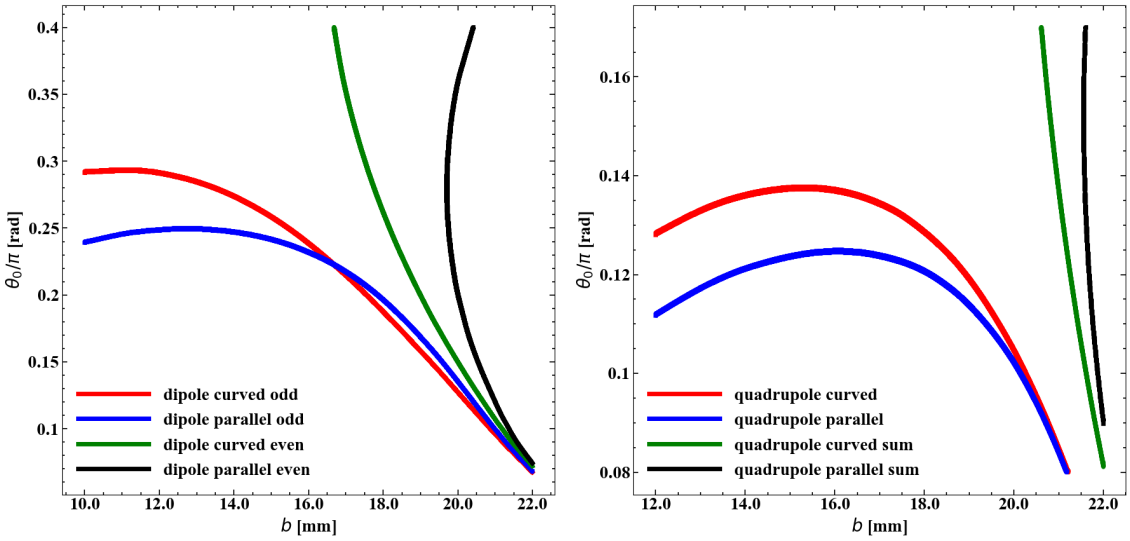

Figure 6: Left: b and θ_0 value at $Z = 50\Omega$ for dipole (all modes). Right: b and θ_0 at $Z = 50\Omega$ for quadrupole (all modes). These are the "possible parameters" we can choose to build the kickers.

5.4 Field quality comparison

External voltages are applied in the dipole odd mode and in the quadrupole mode only, so we need to consider the field quality on axis for these modes only.

A comparison between curved plates and parallel plate is shown in figure 7. We see that in the dipole case for the same b and θ_0, parallel plates have higher central electric field. However, if the shortest distance from the beampipe center to the plate is matched, the curved plate have a slightly higher field at the center. Parallel plates always produce a more uniform field than curved plates.

In the quadrupole case the central field gradient is similar for both parallel and curved plate with the same parameters of b and θ_0; and that the field gradient increases as b decreases.

5.5 Electric field quality at matched characteristic impedance

Using the study above, we looked at the electric field (or field gradient) as a function of b and θ_0 at the matched characteristic impedance. The result is shown in figure 8. The field is taken at $(x = 0, y = 0)$, the center of the kicker and the field gradient is taken to be average field gradient one millimeter on each side from the center $(E_x(x = -1, y = 0) - E_x(x = 1, y = 0))/2$. The quadrupole electric field gradient plots have numerical artifacts because of numerical effects in FEMM. The two intersections of each horizontal line denotes one electric field (or field gradient) and a b and θ_0 value it corresponds to. Depending on the requirement of the electric field, we can find the parameter space where the design meets both the field requirement and characteristic impedance requirement.

We see that for the field in the dipole curved plate to be greater then $100V_p/m$, $b \leq\sim 14$ mm; while for the dipole parallel plate field to be greater then $100V_p/m$, $b \leq\sim 16.5$ mm, while $\theta_0 \sim 0.22\pi$, which corresponds to a shortest distance ~ 13 mm. In the quadrupole case, for the field gradient to be higher then $15000V_p/m^2$, $b \leq\sim 15$ mm with curved plates while with parallel plates for the same field gradient, $b \leq\sim 16$ mm which with $\theta_0 \sim 0.13\pi$, corresponds to a shortest distance of ~ 14.7 mm. To get a strong field (field gradient) at the center, we require the plates to be close to the center.

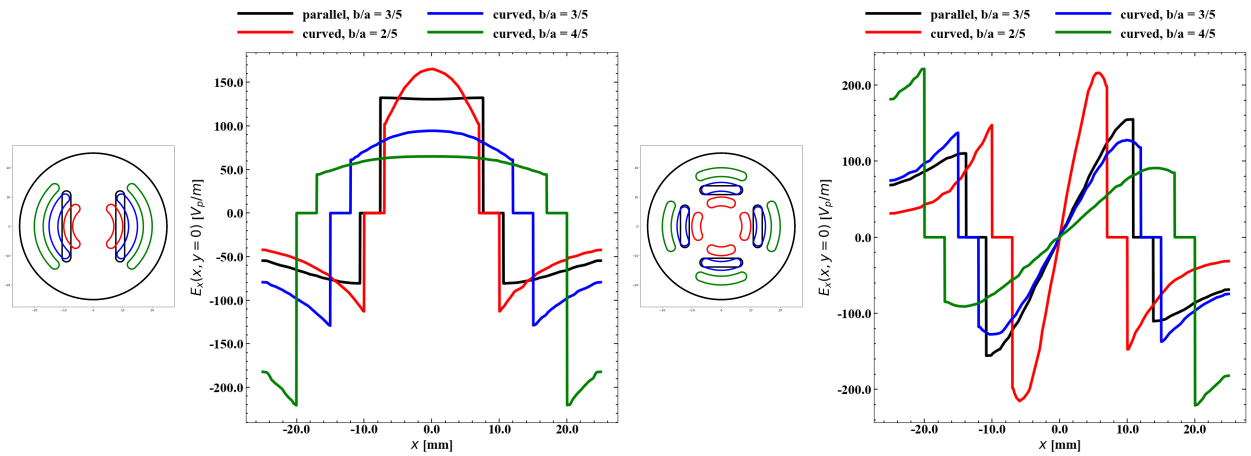

Figure 7: Left: dipole schematic with different plate sizes and shapes and dipole odd mode electric field lineout at $y = 0$, $-a \leq x \leq a$; Right: quadrupole schematic with different plates and quadrupole mode electric field (Ordering of the plate is the same as in figure 1), lineout at $y = 0$, $-a \leq x \leq a$. In our case $a = 25$ mm. The steps corresponds to regions inside the plate, where the electric field inside a conductor is always 0.

5.6 Effect of plate thickness on characteristic impedance

Plate thickness is the parameter that has the weakest influence among the three parameters (b, θ_0 and thickness) considered; nevertheless it has to be taken into account. A comparison is shown in figure 9. From the first row (dipole comparison) we see that the thickness dependence is larger at small θ_0, nevertheless the feasible parameter space of (b, θ_0) for dipole even mode is similar in all cases.

For the quadrupole, the dependence on thickness is stronger then for the dipole case. From the left two figures of the second row, we see that in the quadrupole mode, the dependence on thickness is significant, but in the quadrupole sum mode, the dependence is significantly weaker, especially at large θ_0. This shows that for quadrupole case, thickness is a more important factor then dipole case.

6 CONCLUSIONS

In this project we developed a theory for dipole and quadrupole stripline kickers and examined the electric field quality and characteristic impedance associated with different modes. The semi-analytic solvers we developed produces results in agreement with FEMM except at the immediate vicinity of the plate tips. The discrepancy is likely due to the fact that FEMM cannot accurately model singular behavior near a sharp edge using polynomial interpolation. The semi-analytic solution can be used to determine both the electric field on axis as well as the characteristic impedance.

We used FEMM to model plates with more realistic shapes. We find that for dipoles, parallel plates produces a much more uniform field. With quadrupoles the difference between the curved and parallel plates is not significant at the center; however the field is stronger as the plate gets close to the center. We also investigated the parameter space (plate spacing and coverage angle) that corresponds to a fixed matched impedance value. We found that in general for both dipoles and quadrupoles, the curved plates allow a larger range of values of the plate spacing then the parallel plates. The characteristic impedance dependency on thickness is much stronger for the quadrupole than for the dipole kicker.

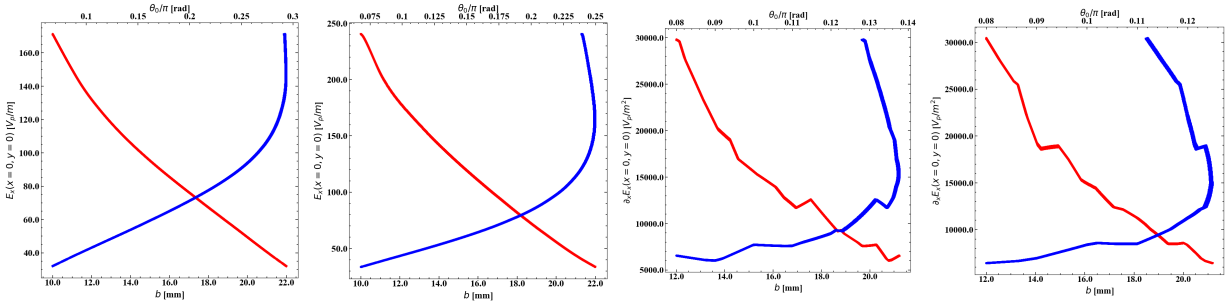

Figure 8: Electric field or field gradient as a function of b and θ_0. Red line corresponds to b and the blue line corresponds to θ_0. The two intersections of each horizontal line denotes one electric field (or field gradient) and the corresponding values of b and θ_0. The quadrupole lines are not strictly monotonic because of numerical effects from FEMM. Left to right: dipole curved plate electric field, dipole parallel plate electric field, quadrupole curved plate electric field gradient and quadrupole parallel plate electric field gradient.

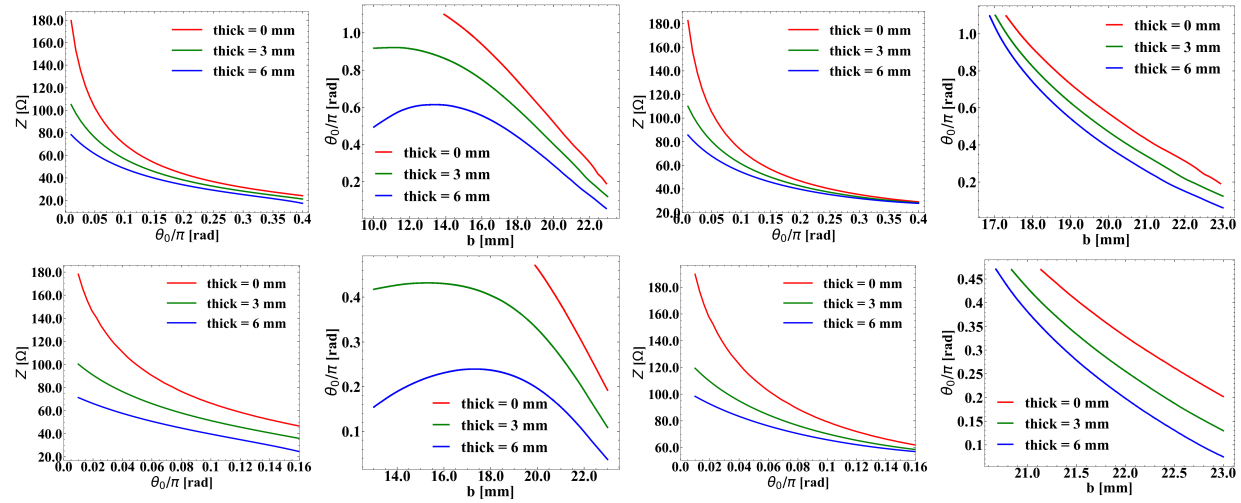

Figure 9: Effect of thickness in kickers. First row left to right, respectively: Dipole odd mode characteristic impedance as a function of θ_0 at $b = 20$ mm; Dipole odd mode $b - \theta_0$ parameter space at $Z = 50\Omega$; Dipole even mode characteristic impedance as a function of θ_0 at $b = 20$ mm; Dipole even mode $b - \theta_0$ parameter space t $Z = 50\Omega$. Second row from left to right, respectively: Quadrupole mode characteristic impedance as a function of θ_0 at $b = 20$ mm; Quadrupole mode $b - \theta_0$ parameter space at $Z = 50\Omega$; Quadrupole sum mode characteristic impedance as a function of θ_0 at $b = 20$ mm; Quadrupole sum mode $b - \theta_0$ parameter space at $Z = 50\Omega$

References

[1] T. Sen, Y. Tu and J.-F Ostiguy, *Fields and Characteristic Impedances of Dipole and Quadrupole Stripline Kickers*, PUB-19-421-AD, FNAL, Batavia, IL, USA (in preparation)

[2] David Meeker, *Finite Element Method Magnetic*. Available at http://www.femm.info/wiki/HomePage